Propagation of transverse domain walls in homogeneous magnetic nanowires

S. Allende, D. Altbir, E. Salcedo, M. Bahiana, and J. P. Sinnecker

Propagation of transverse domain walls in homogeneous magnetic nanowires

S. Allende,[1,a)] D. Altbir,[1] E. Salcedo,[1,2] M. Bahiana,[3] and J. P. Sinnecker[3]

[1]*Departamento de Física, Universidad de Santiago de Chile, USACH, Av. Ecuador 3493, Santiago, Chile*
[2]*Instituto de Física, Universidade Federal do Rio Grande do Sul, CP 15051, 91501-970 Porto Alegre, Rio Grande do Sul, Brazil*
[3]*Instituto de Física, Universidade Federal do Rio de Janeiro, CP 68528, 21941-972 Rio de Janeiro, Brazil*

The field driven nucleation and propagation of transverse domain walls in a uniform Ni nanowire is examined by means of Monte Carlo simulations combined with a scaling technique. Simulations show a nonlinear behavior followed by the simultaneous nucleation of several domain walls. Also we study the angular dependence of the propagation of the transverse domain wall with external field. Results are analyzed in terms of the classical relaxation model for interface dynamics. © *2008 American Institute of Physics.* [DOI: 10.1063/1.2939264]

I. INTRODUCTION

The field driven reversal processes in nano- and microwires have been extensively studied with a variety of theoretical and experimental techniques due to its relation to the performance of magnetic storage and spintronic devices.[1] The wires considered in the literature may be broadly classified according to their geometric parameters (diameters in the nano- or micrometer scale and aspect ratio), constituting material (pure substance, alloy, etc.), and interactions (isolated or embedded in dense arrays). All these characteristics may influence the overall reversal process, impeding the isolation of the basic principles behind the observed behaviors.

Although the reversal process in isolated nanowires has been addressed analytically in works dating as early as 1958,[2] an experimental realization has become possible only about ten years ago with the advances in the fabrication of nanostructured materials and measurements of low magnetization values.[3] Wernsdorfer *et al.*[4,5] studied the behavior of the switching field in single Ni nanowires, as a function of temperature and field sweeping rate, for wires with diameter ranging from 40 to 100 nm and lengths up to 5 μm. For the narrower wires, the estimated activation volume for reversal was two orders of magnitude smaller than the cylinder volume, leading the authors to conclude that the reversal of magnetization was caused by nucleation of a reversed fraction of the cylinder, rapidly propagating along the sample. Nucleation of domain walls was also observed by Paulus *et al.*[6] in arrays of noninteracting Ni nanowires with diameters in the range of 6–50 nm.

The theoretical modeling of these systems is by no means trivial, since the internal structure of the wire must be considered, which means dealing with long range dipolar interactions besides the exchange coupling. Braun[7–9] performed detailed analytical investigations of the switching rate and energy barriers involved in the reversal process of uniform nanowires. His main result is that, in nanowires whose length exceeds the width of a static domain wall, thermal magnetization reversal occurs via formation of domain wall pairs of opposite chirality, also known as soliton-antisoliton pairs, with an activation energy proportional to the cross-sectional area of the wire, leading to coercivity values much smaller than the ones predicted by uniform rotation. Micromagnetic simulations have been used by Hertel and Kirschner[10] to investigate the structure of the wall in the reversal process in Ni nanowires with diameters of 30–60 nm and lengths of 1 μm. By considering a cone-shaped wire, they observed that the reversal mode changed from corkscrew to curling as the wire radius increases beyond a critical value. Also, depending on the diameter of the nanowire, Wieser *et al.*[11] observed two different reversal modes for nanowires, a transverse and a vortex wall. Forster *et al.*[12] observed the same behavior in Co nanowires. In this work, the velocity of propagation of the domain wall is proportional to the applied field. The mechanism of nucleation and propagation of a single-domain wall was studied as a function of temperature in a bistable Fe-based amorphous microwire with a unique simple domain structure by Varga *et al.* From a quantitative analysis of the propagating wall characteristics, the authors proposed a damping mechanism which dominates in the low temperature regime.[13]

In a previous work, Bahiana *et al.*,[14] by means of a scaling technique,[15] investigated the reversal mechanisms of an interacting hexagonal array of wires. Different reversal modes were observed as a function of the dipolar interactions between the wires. In particular, the nucleation of domain walls was identified as the main mechanism for magnetization reversal. In this paper, we consider a simpler system in order to examine the reversal process in its fundamental essence. Our choice is a single nickel nanowire subjected to an applied field. Since nickel appears in a fcc lattice, the contribution of crystalline anisotropy is very small and can be safely neglected. Our goal is to examine the nucleation and propagation of domain walls as a function of the applied field and analyze its dynamics in terms of the classical relaxation model for interface dynamics.[16] Simulation results show the appearance of a nonlinear regime, precursor of one in which several domains nucleated at the same time.

---

a)Electronic mail: sallende@fisica.usach.cl.

© 2008 American Institute of Physics

II. MODEL

Our starting point is a uniform Ni nanowire with diameter $d = 30$ nm and length $\ell = 500$ nm, built along the [001] direction of a fcc lattice with parameter $a_0 = 3.52$ Å. The energy of each magnetic moment **m** can be written as

$$E = -\mathbf{m} \cdot \mathbf{B}_{eff}, \tag{1}$$

where $\mathbf{B}_{eff}$ is the effective field including contributions from the applied field ($\mathbf{B}_a$), exchange ($\mathbf{B}_x$), and dipolar interactions ($\mathbf{B}_d$) in the form

$$\mathbf{B}_{eff} = \mathbf{B}_a + \mathbf{B}_x + \mathbf{B}_d = \mathbf{B}_a + J \sum_{i \in \{nn\}} \mathbf{m}_i$$

$$+ \sum_i \frac{3(\mathbf{m}_i \cdot \hat{n}_i)\hat{n}_i - \mathbf{m}_i}{r_i^3}, \tag{2}$$

where J is the exchange coupling constant, $\{nn\}$ the set of nearest neighbors, r_i the distance to the ith atom, and $\hat{n}_i$ the unitary vector along $\mathbf{r}_i$. The saturation value of **m** is $m = 0.615\mu_B$ and the exchange coupling constant $J = 1600$ kOe$/\mu_B$.[17,18] Such wire contains about 6×10^9 atoms, which is out of reach for a regular Monte Carlo simulation with dipolar interactions, considering the available computational power. In order to reduce the number of interacting atoms, we make use of a scaling technique, proposed by d'Albuquerque e Castro *et al.*,[15] originally formulated to investigate the equilibrium phase diagram of cylindrical particles of height h and diameter d. The authors showed that this diagram is equivalent to that for a smaller particle with $d' = d\chi^\eta$ and $h' = h\chi^\eta$, with $\chi < 1$ and $\eta \approx 0.56$, if the exchange constant is also scaled as $J' = \chi J$. It has also been shown[19] that the scaling relations can be used together with Monte Carlo simulations to obtain a general magnetic state of a nanoparticle. We use this idea starting from the desired value for the total number of interacting particles we can deal with, based on the computational facilities currently available, and have estimated $N \approx 3000$. With this in mind, we have obtained the scale value $\chi = 4 \times 10^{-3}$, leading to a wire with 2835 atoms. In its original formulation, the scaling technique did not include temperature. However, since thermal activation is a key issue for transitions between metastable states and the energy landscape depends on the value of χ, temperature must also be scaled. Although temperature scaling is still an open issue, we considered that even if the energy landscape is rather complicated due to the dipolar interaction, in the vicinity of each local minimum we can analyze the transitions as regulated by simple energy barriers of the form $K_e V_e$, where K_e is an effective anisotropy constant taking into account several energy contributions, and V_e is an effective volume. Thermally activated transitions naturally lead to the definition of a blocking temperature $T_B \propto K_e V_e$,[20] so we use this to relate temperature and size. In order to keep the thermal activation process invariant under the scaling transformation, the energy barriers must also be invariant; therefore, the temperature should scale as the volume, that is, $T' = \chi^{3\eta}T$. This technique was presented by Vargas *et al.*[19] and has been used before to investigate magnetic dots,[21] tubes,[22] and wires,[14] showing good agreement with experiments or micromagnetic calculations.
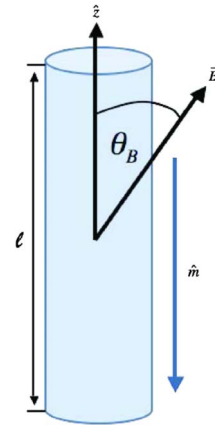

FIG. 1. (Color online) Definition of relevant geometrical parameters. The orientations of magnetization and external field correspond to a typical initial condition.

Monte Carlo simulations were carried out at $T = 300$ K using regular Metropolis algorithm.[23] The new orientation of a magnetic moment was chosen arbitrarily with a probability $p = \min[1, \exp(-\Delta E/k_B T)]$, where ΔE is the change in energy due to the reorientation of the magnetic moment and k_B is the Boltzmann constant. Results presented in this paper correspond to an average of 10–20 independent realizations.

III. RESULTS AND DISCUSSION

The geometry used in the simulations is illustrated in Fig. 1. The initial state has the magnetization saturated in the $-z$ direction, with the external field applied at an angle θ_B. Due to strong stray fields, the domain structure at the wire tips are usually composed of several closure domains. If allowed to relax, magnetization reversal may occur through the propagation of a pair of domain walls nucleated at the tips.[14,24] In an experimental setup, this could affect measurements of domain wall propagation time, in which case it is useful to inhibit the propagation of one of the domain walls by, for example, placing one of the wire tips outside the external field region,[25] or to induce the nucleation in one particular tip by increasing the value of the applied field near that tip. In order to optimize the simulation, we followed the first procedure, inhibiting the nucleation at one of the wire tips by choosing $B_a = 0$ for the atoms in the last 12 nm. The reversal process was monitored by the values of $\mu_i(z) \equiv \bar{m}_i/m$, $i = x, y, z$, which are the average values of magnetic moment components relative to its saturation value. For some range of parameters, it is easy to identify the domains with $\mu_z(z) = \pm 1$, separated by an interface or domain wall. The position of the wall z_w may be determined by the maximum of $(1 - |\mu_z|)$, as shown in Fig. 2. In this particular case, a wall located at $z_w = 240$ nm with thickness $\delta \approx 40$ nm can be clearly identified. The wall thickness is defined as the width of the region where μ_z is within 85% of the saturation value. In this scenario, one may reduce the problem of the individual reversal of atomic moments to the one-dimensional motion of a domain wall.

Depending on the value of θ_B, different reversal modes are observed. Figure 3 shows typical magnetization profiles for $\theta_B = 0°$, 15°, and 30°, obtained at two different moments
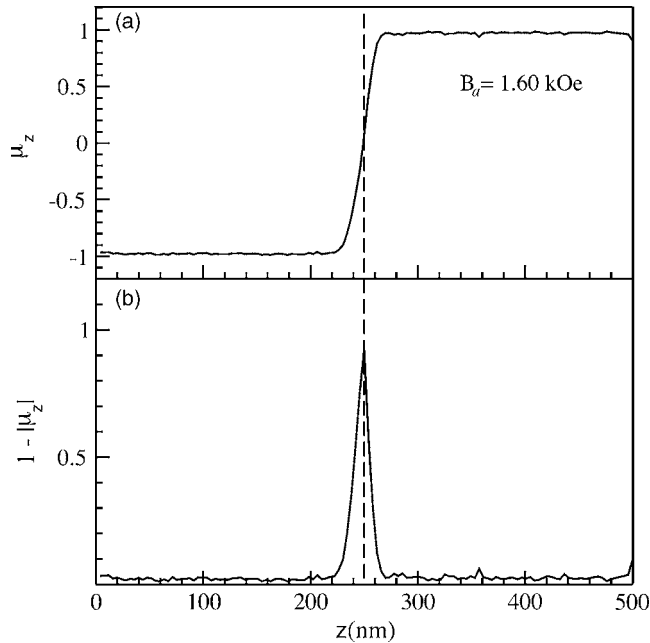
FIG. 2. Typical magnetization profile for B_a=1.6 kOe: (a) $\mu_z(z)$ and (b) $(1-|\mu_z|)$. In this case, it is easy to identify a domain wall centered at z_w =250 nm. Magnetization behind and ahead of the wall is homogeneous, and the reversal process may be described by means of $z_w(t)$.

of the reversal process. For $\theta_B=0°$ [Fig. 3(a)], the reversal process occurs by means of a corkscrew mode,[10] in which the magnetic moments inside a region with finite width reverse their direction, along a given plane containing the wire axis. This plane rotates around the wire axis as the wall propagates, as can be seen by the $\mu_x(z)$ and $\mu_y(z)$ profiles at different points of the wall trajectory. When $\theta_B \neq 0$, the torque due to the xy components of the field causes a rotation
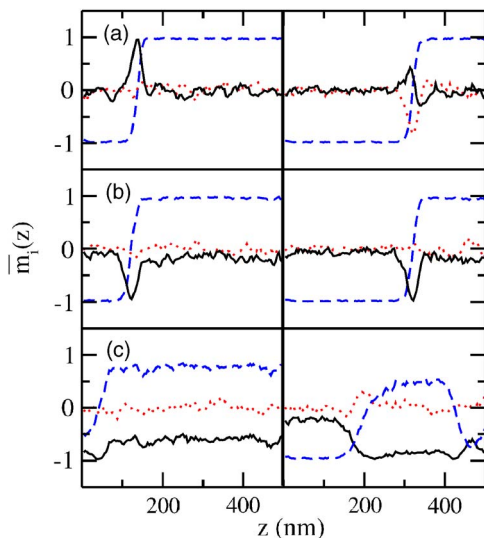

FIG. 3. (Color online) Snapshots of the magnetization profile at two different moments of the reversal process, with B_a=1.6 kOe. Dashed line: $\bar{m}_z$, dotted line: $\bar{m}_x$, and solid line: $\bar{m}_y$. (a) $\theta_B=0°$: corkscrew reversal mode. The x and y profiles change with time, indicating that the wall plane rotates around the z axis. (b) $\theta_B=15°$: transverse reversal mode. Magnetization profile in all directions presents the same shape, corresponding to the average components in the plane defined by the z axis and B_a. (c) $\theta_B=30°$: multidomain reversal. The wall structure is lost during propagation due to the formation of multiple domains along the wire.

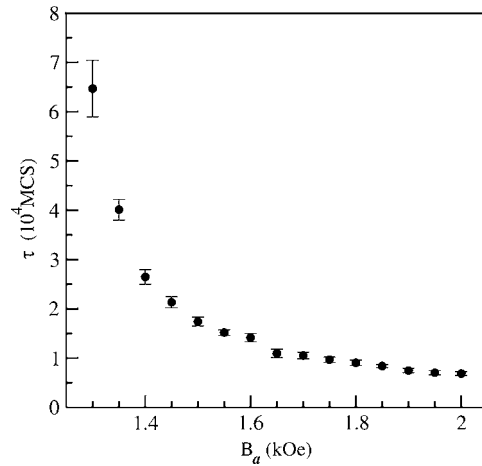FIG. 4. Waiting times for different values of the applied field. Here θ_B =0°.

of the magnetic moments, affecting the reversal mode. In this case, we identify three different reversal modes, regarding both field intensity and θ_B: corkscrew, transverse [Fig. 3(b)], and multidomain [Fig. 3(c)]. The transverse reversal mode is similar to the corkscrew mode, but with the domain wall on a fixed plane defined by the applied field and the nanowire axis. In the multidomain reversal mode, there are two or more domain walls in the wire.

Although not corresponding to an equilibrium state, the initial configuration may persist for some time due to its degree of metastability for weak applied fields. We defined the waiting time τ as the time, measured in Monte Carlo steps (MCSs), before which the wire magnetization had decreased to 90% of its saturation value for a fixed external field.

A. Propagation with $\theta_B=0°$

First we examine the effect of the field strength on the waiting time for the wall nucleation. Figure 4 shows the values of τ for different applied fields. From this figure it is possible to verify that, for fields below 1.3 kOe, the formation of a domain wall is not only difficult, due to the long waiting times involved, but extremely affected by thermal fluctuations. In order to avoid long waiting times, the nucleation of walls at low fields was boosted by the application of a field pulse, following an experimental procedure described by Beach *et al.*[26] In our case, the pulse consisted in the application of a higher field of 2.0 kOe until the wall had reached the position z_w=100 nm, then the propagation of the wall followed with a weaker applied field, corresponding to the indicated B_a in the following discussion. With this procedure we were able to monitor the propagation of walls for fields as low as 0.25 kOe. Figure 5 shows a typical plot of z_w as a function of time, in MCS, for B_a=1.6 kOe. The velocity of the wall may be directly calculated from the slope obtained by a linear fitting of the data.

For fields in the range $0.25 \leqslant B_a \leqslant 2.4$ kOe, we found the propagation to occur always at constant speed, characterizing a viscous regime.[27] In this case, the response of the domain wall to a weak applied field may be described by the classi-
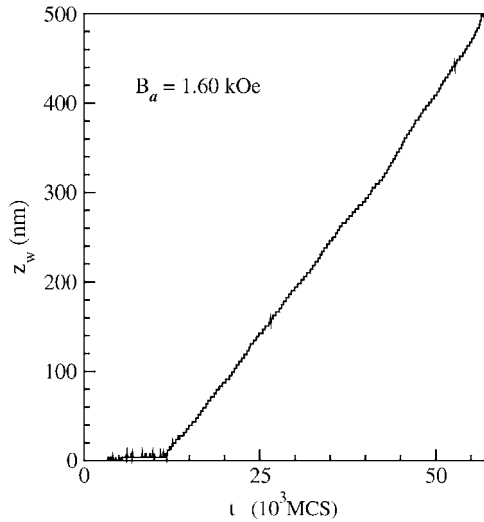
FIG. 5. Wall position as a function of time.

cal equation of motion for an overdamped oscillator,[18] leading to the expression for the steady state wall velocity v:

$$v = S(B_a - B_0), \tag{3}$$

where S is the mobility, and B_0 a parameter usually obtained by fitting of data, measured with an applied field larger than a certain depinning value, extrapolated to the $v=0$ point.[16,18] We checked the validity of Eq. (3) by calculating the wall velocity for different values of applied field. The results are shown in Fig. 6, together with the values of the energy dissipation rate due to the relaxation process. Three regimes may be identified in this figure:

(1) $0.25 \text{ kOe} \lesssim B_a \lesssim 1.3 \text{ kOe}$—linear regime, a field pulse is needed to nucleate the wall, which moves at constant speed afterwards.

(2) $1.3 \text{ kOe} \lesssim B_a \lesssim 1.7 \text{ kOe}$—linear regime, the domain wall nucleates spontaneously, and propagates at constant speed.

(3) $1.7 \text{ kOe} \lesssim B_a \lesssim 2.4 \text{ kOe}$—nonlinear regime, the measured velocity is larger than the value extrapolated from the previous linear region. At this field value, the wall loses its rigidity along propagation.
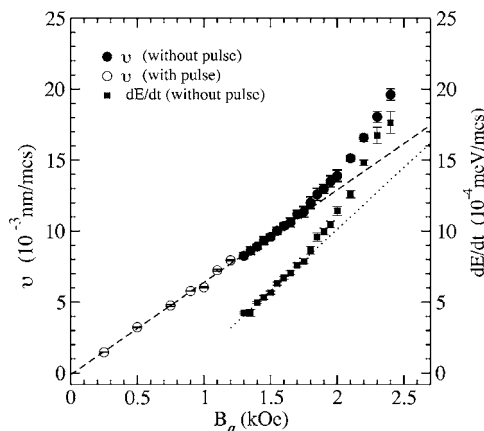

FIG. 6. Energy dissipation rate (right axis, squares) and wall velocity (left axis, circles) as a function of applied field. Open symbols correspond to propagation boosted by a field pulse.
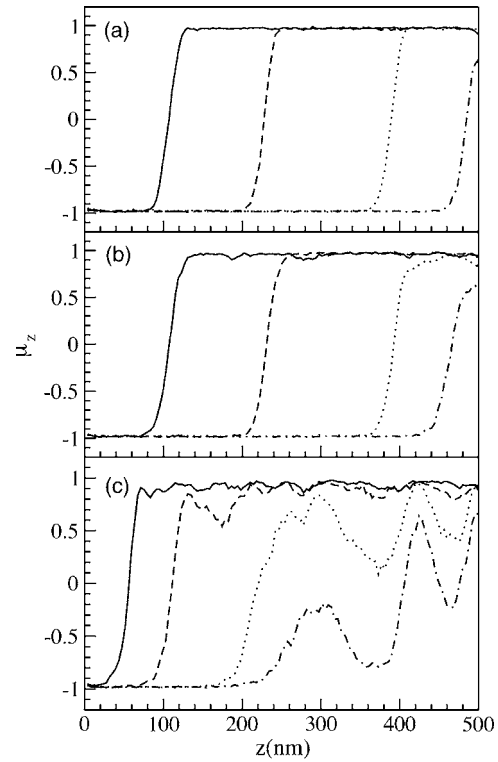

FIG. 7. Magnetization profile for (a) $B_a=1.3$ kOe,(b) $B_a=2.4$ kOe, and (c) $B_a=3.0$ kOe. Distinct line styles illustrate different stages of the wall propagation along the wire. For fields $B_a \gtrsim 2.4$ kOe, the region immediately in front of the wall becomes unstable, and for $B_a \gtrsim 3.0$ kOe reversed domains nucleate ahead.

In order to understand the nonlinear region, we compared the magnetization profile for certain values of B_a. Figure 7 shows snapshots of the domain wall, at different points along the wire, for $B_a=1.3$, 2.4, and 3.0 kOe. For $B_a=1.3$ kOe [Fig. 7(a)], propagation is in the beginning of the second linear regime. Regions behind and in front of the wall are saturated and uniform, and the wall is well defined, with thickness $\delta=40$ nm. The same behavior is observed for all field values in the second linear region. $B_a=2.4$ kOe [Fig. 7(b)], corresponds to the nonlinear region. In this case, we observe fluctuations in the magnetization values in front of the wall, which is thicker, with $\delta \approx 55$ nm. Still, the definition of a domain wall, with associated position and velocity, is possible. Finally, for $B_a=3.0$ kOe, the uniform state is unstable ahead of the wall, and several domain walls are formed, as can be seen in Fig. 7(c).

B. Propagation with $\theta_B \neq 0°$

In order to better understand the process of magnetization reversal for fields with $\theta_B \neq 0°$, we divide it into three stages. In the first one, the magnetic moments rotate until they form some angle with the z axis. The movement is induced by a torque of the xy components of the applied field and the low demagnetizing field on that plane. We call it the redirection stage. The redirection of the moments brings a decrease in the shape anisotropy along the wire axis, making the nucleation easier. The second stage corresponds to the nucleation of the domain wall and strongly depends on the
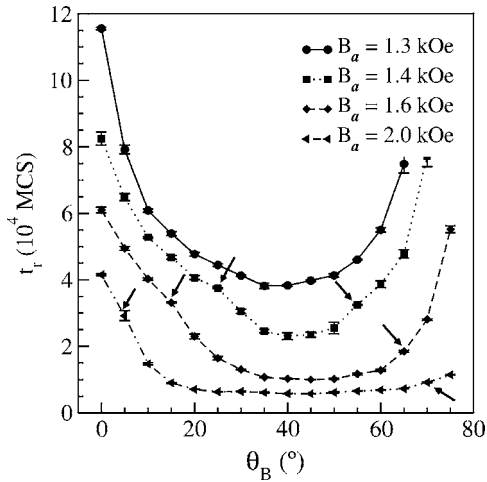
FIG. 8. Magnetic reversal time as a function of the applied field angle θ_B for different field values. Values of t_r represent averages over six realizations. The arrows delimitate regions in which multiple domain wall formation is observed.

magnitude of the z component of the applied field, as in the $\theta_B = 0°$ case. The last stage corresponds to the propagation of the already formed domain wall. We define the reversal time t_r as the sum of the times involved in these three stages. Figure 8 shows the dependence of the average reversal time on θ_B for different values of the applied field. From $\theta_B = 0$ to $\theta_B \sim 45°$, t_r continuously decreases, reaching a minimum or a plateau, corresponding to an optimal combination of the redirection, nucleation, and propagation stages for those values of θ_B. For $B_a = 1.3$ kOe, all values of θ_B lead to the formation and propagation of one single wall. In this case, the propagation speed is well defined and depends on θ_B, as shown in Fig. 9. For $B_a = 1.4$ kOe, when $20° \lesssim \theta_B \lesssim 60°$ multiple domain walls are nucleated, decreasing considerably the value of t_r. The same behavior is observed for larger values of the applied field, for angles in the intervals indicated by arrows in the figure. As the field increases, the range of angle values for multiple nucleation also increases. Along a given $t_r(\theta_B)$ line, for $B_a \geq 1.4$ kOe four different regimes are observed. Taking, for example, the curve for $B_a = 1.6$ kOe, we have that for small angles, $\theta_B \lesssim 5°$, propagation is via a corkscrew reversal mode. As the perpendicular component increases, for
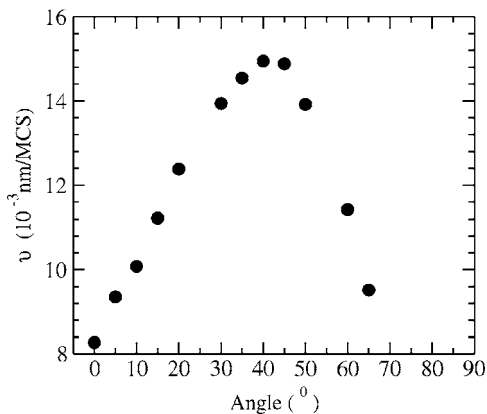
$5° \lesssim \theta_B \lesssim 15°$, the reversal plane becomes fixed, and the transverse mode is established, with a single wall propagation. A further increase in θ_B leads to a third region, $15° \lesssim \theta_B \lesssim 20°$, with reversal in the transverse mode, but with a second domain wall nucleated at the other tip. For $20° < \theta_B < 65°$, the reversal of the magnetization nucleates at different parts of the wire. In the neighborhood of $\theta_B \sim 45°$, after the activation of the magnetic reversal at the most favorable tip for this process, the reversal follows, generating an almost coherent process along all the wires (see Fig. 3(c)). Finally, for $\theta_B \gtrsim 45°$, the decrease in the parallel component of the field leads to larger values of t_r due to a significant increase in the nucleation time.

IV. CONCLUSION

We have used Monte Carlo simulations combined with a scaling technique in the theoretical investigation of domain wall propagation in homogeneous nickel nanowires. With this approach, we were able to systematically calculate the domain wall velocity and found different propagation regimes as the applied field strength and direction were varied. For fields parallel to the wire axis we found that, for low and intermediate fields, the nucleation of a reversed domain requires an amount of time that rapidly increases as the applied field is decreased. This is not an effect of disorder, since the system is a perfect crystal, it appears uniquely due to the existence of a field dependent energy barrier between states with negative and positive magnetizations. From 0.25 to 1.7 kOe, the propagation occured always with constant speed. The velocity varied linearly with the applied field, in agreement with the classical picture of viscous relaxation,[16] and the wall thickness was approximately 40 nm. For larger fields, up to 2.4 kOe, we found a nonlinear behavior with a velocity higher than the value extrapolated from the linear relation for lower fields. The domain wall thickness in this region continuously increases up to $\delta = 55$ nm for $B_a = 2.4$ kOe. It is possible to cast the results from Fig. 6 into the relaxation relation (3) if a field dependent mobility is defined. In the context of one-dimensional wall propagation in crystalline ferromagnetic media, a simple model, taking into account exchange and crystalline anisotropy energies only,[13] predicts a domain wall mobility in the form

$$S \propto \delta, \tag{4}$$

due to the fact that the domain wall mobility is $S = 2M_s/\beta$, where M_s is the saturation magnetization and β is the domain wall damping given only by the contribution of the spin-relaxation damping coefficient. This coefficient is proportional to M_s/δ. The thickness of the wall may be calculated by energy minimization,[28] leading to a general form $\delta \propto \sqrt{J/K}$. Here K is a uniaxial anisotropy constant, usually assumed to be of crystalline origin. In this picture, given a certain material, once M_s, K, and J are fixed (at least in an average sense), the wall velocity is determined, independent of the applied field. Our simulations showed that, for large enough fields (>1.7 kOe), the measured velocity is higher than the value predicted by the linear relation. Consistently,

FIG. 9. Domain wall propagation speed as a function of θ_B for $B_a = 1.3$ kOe.

the value of δ in that range of fields, measured directly from the magnetization profile, increases. We interpret these results by defining a $K(B)$ or field dependent anisotropy constant. Our simulations do not include crystalline anisotropy, so the only source of anisotropy is the shape or the presence of a demagnetizing field. Fluctuations around the uniform state affect the demagnetizing field, decreasing it. For $B_a > 2.4$ kOe, this effect destroys the stability of the inverted domain ahead of the wall. We checked this hypothesis by introducing an arbitrary uniaxial anisotropy along the propagation direction. Simulation results showed that the propagation velocity linearly decreases with the increase in anisotropy constant. For an applied field of 2.4 kOe, the anisotropy constant needed for propagation, with the speed predicted by the viscous regime, is 5.3×10^6 erg/cm^3, much larger than the value usually attributed to nickel.

The behavior of the reversal time as θ_B is varied (Fig. 8) may be compared to the one obtained by Wernsdorfer *et al.* for the switching field in an experiment with a single nickel nanowire with $d=50$ nm.[5] The increase in the switching field for $\theta_B=0°$ and $\theta_B=90°$, predicted by the coherent rotation model, is consistent with the increase in the overall reversal time observed in our simulations.

ACKNOWLEDGMENTS

[1] D. A. Allwood, G. Xiong, C. C. Faulkner, D. Atkinson, D. Petit, and R. P. Cowburn, Science **309**, 1688 (2005).

[2] A. Aharoni and S. Shtrikman, Phys. Rev. **109**, 1522 (1958).

[3] B. Barbara, Solid State Sci. **7**, 668 (2004).

[4] W. Wernsdorfer, K. Hasselbach, A. Benoit, B. Barbara, B. Doudin, J. Meier, J.-Ph. Ansermet, and D. Mailly, Phys. Rev. B **55**, 11552 (1997).

[5] W. Wernsdorfer, B. Doudin, D. Mailly, K. Hasselbach, A. Benoit, J. Meier, J.-Ph. Ansermet, and B. Barbara, Phys. Rev. Lett. **77**, 1873 (1996).

[6] P. M. Paulus, F. Luis, M. Kröll, G. Schmid, and L. J. de Jongh, J. Magn. Magn. Mater. **224**, 180 (2001).

[7] H.-B. Braun, Phys. Rev. Lett. **71**, 3557 (1993).

[8] H.-B. Braun, J. Appl. Phys. **76**, 6310 (1994).

[9] H.-B. Braun, J. Appl. Phys. **99**, 08F908 (2006).

[10] R. Hertel and J. Kirschner, Physica B **343**, 206 (2004).

[11] R. Wieser, U. Nowak, and K. D. Usadel, Phys. Rev. B **69**, 064401 (2004).

[12] H. Forster, T. Schrefl, W. Scholz, D. Suess, V. Tsiantos, and J. Fidler, J. Magn. Magn. Mater. **249**, 181 (2002).

[13] R. Varga, K. L. Garcia, M. Vázquez, and P. Vojtanik, Phys. Rev. Lett. **94**, 017201 (2005).

[14] M. Bahiana, F. S. Amaral, S. Allende, and D. Altbir, Phys. Rev. B **74**, 174412 (2006).

[15] J. d'Albuquerque e Castro, D. Altbir, J. C. Retamal, and P. Vargas, Phys. Rev. Lett. **88**, 237202 (2002).

[16] A.-L. Barabási and H. E. Stanley, *Fractal Concepts in Surface Growth* (Cambridge University Press, Cambridge, England, 2004).

[17] C. Kittel, *Introduction to Solid State Physics* (Wiley, New York, 2004).

[18] G. Bertotti, *Hysteresis in Magnetism. For Physicists, Materials Scientists, and Engineers* (Academic, New York, 1998).

[19] P. Vargas, D. Altbir, and J. d'Albuquerque e Castro, Phys. Rev. B **73**, 092417 (2006).

[20] B. D. Cullity, *Introduction to Magnetic Materials* (Addison-Wesley, Reading, MA, 1972).

[21] J. Mejía-López, D. Altbir, A. H. Romero, X. Batlle, V. Roshchin, C.-P. Li, and I. K. Schuller, J. Appl. Phys. **100**, 104319 (2006).

[22] P. Landeros, S. Allende, J. Escrig, E. Salcedo, D. Altbir, and E. E. Vogel, Appl. Phys. Lett. **90**, 102501 (2007).

[23] K. Binder and D. W. Heermann, *Monte Carlo Simulation in Statistical Physics* (Springer, New York, 2002).

[24] T. Reininger, H. Kronmuller, C. Gomezpolo, and M. Vazquez, J. Appl. Phys. **73**, 5357 (1993).

[25] R. Novak (2005). M.S. thesis, UFRJ, 2005.

[26] G. S. D. Beach, C. Nistor, C. Knutson, M. Tsoi, and J. L. Erskine, Nature (London) **4**, 741 (2005).

[27] R. Ferré, K. Ounadjela, J. M. George, L. Piraux, and S. Dubois, Phys. Rev. B **56**, 14066 (1997).

[28] C. Kittel, Rev. Mod. Phys. **21**, 541 (1949).